Interface Magnetoelectric Coupling in $Co/Pb(Zr,Ti)O_3$

Ondřej Vlašín[1], Romain Jarrier[1], Rémi Arras[2], Lionel Calmels[2], Bénédicte Warot-Fonrose[2], Cécile Marcelot[2], Matthieu Jamet[3], Philippe Ohresser[4], Fabrice Scheurer[1], Riccardo Hertel[1,5], Gervasi Herranz[6], Salia Cherifi-Hertel[1,*]

1 Institut de Physique et Chimie des Matériaux de Strasbourg, UMR 7504, CNRS and Université de Strasbourg, 23 rue du Loess F-67300 Strasbourg, France
2 CEMES, Université de Toulouse, CNRS, UPS, 29, rue Jeanne-Marvig, F-31055 Toulouse, France
3 Université Grenoble Alpes and CEA, INAC-SP2M, F-38000 Grenoble, France
4 Synchrotron SOLEIL, L'orme des Merisiers, Saint-Aubin, F-91192 Gif-sur-Yvette, France
5 Karlsruhe Institute of Technology, Physikalisches Institut, Wolfgang-Gaede-Str. 1, 76131 Karlsruhe, Germany
6 Institut de Ciència de Materials de Barcelona (ICMAB-CSIC), Campus de la UAB, Bellaterra 08193, Catalonia, Spain

ABSTRACT

Magnetoelectric coupling at multiferroic interfaces is a promising route towards the nonvolatile electric field-control of magnetization. Here, we use optical measurements to study the static and dynamic variations of the interface magnetization induced by an electric field in $Co/PbZr_{0.2}Ti_{0.8}O_3$ (Co/PZT) bilayers at room temperature. The measurements allow us to identify different coupling mechanisms. We further investigate the local electronic and magnetic structure of the interface by means of transmission electron microscopy, soft x-ray magnetic circular dichroism and density functional theory to corroborate the coupling mechanism. The measurements demonstrate a mixed linear and quadratic optical response to the electric field, which results from a magneto-electro-optical effect. We propose a decomposition method of the optical signal to discriminate between different components involved in the electric field-induced polarization rotation of the reflected light. This allows us to extract a signal that we can ascribe to interface magnetoelectric coupling. The associated surface magnetization exhibits a clear hysteretic variation of odd symmetry with respect to the electric field and nonzero remanence. The interface coupling is remarkably stable over a wide frequency range (1-50 kHz) and the application of a bias magnetic field is not necessary for the coupling to occur. These results show the potential of exploiting interface coupling with the prospect of optimizing the performance of magnetoelectric memory devices in terms of stability, as well as fast and dissipationless operation.

KEYWORDS: magnetoelectrics, artificial multiferroics, interface-mediated coupling, electro-optic effect, magneto-optic effect.

1. INTRODUCTION

Over the last decades, research on spin electronics has been strongly influenced by the discovery of alternative means to control the magnetization, *i.e.*, other than by applying a magnetic field[1,2]. The possibility to control a nanomagnet with an electric current via the spin-transfer torque effect or with an electric field through the magnetoelectric coupling has inspired a considerable amount of technological concepts. Against this backdrop, magnetoelectric materials such as artificial or intrinsic multiferroics are particularly promising, as they provide enhanced magnetoelectric properties that can be addressed at low energy[3–7]. In this context, composite ferromagnetic and ferroelectric systems represent a natural pathway towards the efficient electric-field control of the magnetization at room temperature, owing to converse magnetoelectric coupling (MEC)[8–11]. The electric field control of the magnetic state in multiferroic heterostructures, for instance in ferromagnetic/ferroelectric bilayers, occurs through both, strain-mediated mechanism (converse piezoelectric effect and magneto-elastic interaction) and interface-related effects (electronically driven or via exchange coupling)[11]. The electronically-driven interface coupling[12,13] is particularly interesting for applications[14] as it could be exploited for devices with two-state nonvolatile magnetization, where each state is connected to two opposite ferroelectric polarization orientations[15]. Understanding the details of the coupling effects and their dynamic properties is a major challenge in fundamental material science, and it is of paramount significance for the development of new magnetoelectric devices.

The study of interface-related coupling is difficult as it involves the detection of the variation of the magnetic moment as a function of the external electric field within two or three atomic layers at a buried interface. Transport measurements in multiferroic tunnel junctions containing a ferroelectric barrier have proven to be highly sensitive to interface spin polarization[16] and they have been successfully applied to study various multiferroic heterostructures. Recently, Pantel *et al.* reported an abnormal sign reversal of the tunneling magnetoresistance (TMR) in La(Sr)MnO_3/$PbZr_{0.2}Ti_{0.8}O_3$/Co (LSMO/PZT/Co) upon the polarization reversal of PZT[17]. This result was attributed to the MEC at the Co/PZT interface, while the LSMO/PZT interface was supposed to be passive. A theoretical study of the Co/PZT interface from first-principles calculations revealed that the polarization switching might reverse the spin polarization at the Co/PZT interface[18], which could explain the sign reversal of the TMR in LSMO/PZT/Co tunnel junctions. However, the theoretical study of the spin-dependent tunneling in Co/PZT/Co could not confirm the spin polarization switching at the Co/PZT interface[19]. The high spin polarization of LSMO[20] and the lack of the sign inversion of the TMR in Co/PZT/Co suggest that the LSMO/PZT interface could be magnetoelectrically active in LSMO/PZT/Co tunnel junctions.

In this work, we investigate the MEC in Co/$PbZr_{0.2}Ti_{0.8}O_3$ (Co/PZT) bilayers at room temperature. The origin of the coupling mechanism as well as its statics and dynamics are experimentally studied by means of electric field-modulated optical measurements. The magnetic and electronic structure of the interface are further investigated by means of x-ray magnetic circular dichroism (XMCD) in combination with first-principles calculations. We focus on the optically measured magnetoelectric hysteresis dynamics in the 10^{-1}-10^{4} Hz range. Disentangling the different components, in particular interface coupling, from the complex optical response was one of the main challenges in this study. We propose a generally applicable signal decomposition method to extract the magneto-optical contribution related to interface MEC.

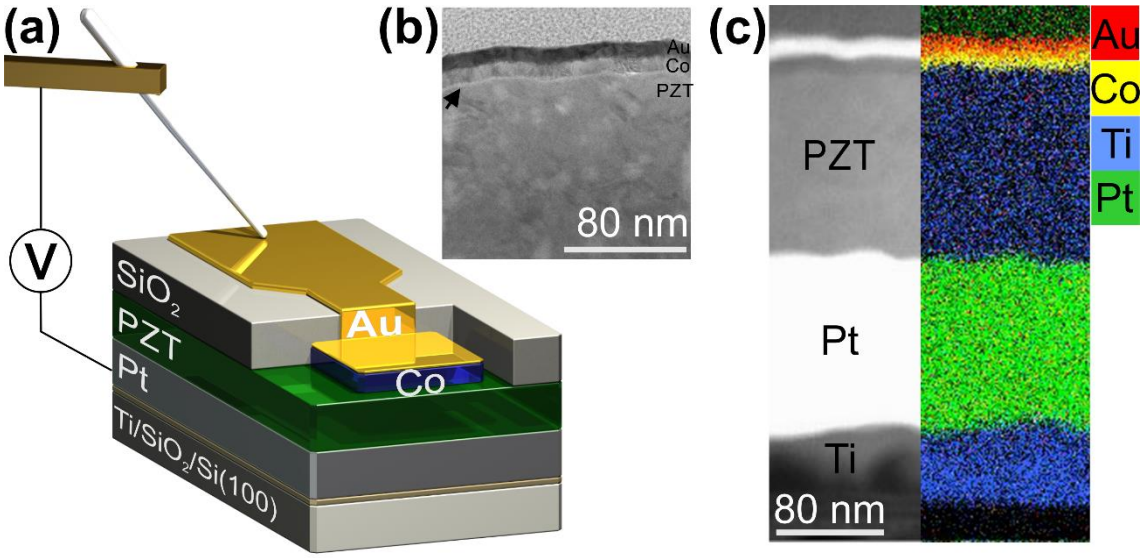

Figure 1. (a) Schematic sample design, (b) high-resolution transmission electron microscopy (TEM) image highlighting a bright interface region (as shown by the arrow), (c) Scanning TEM (STEM) image (left) and the corresponding color-coded chemical analysis (right) obtained by means of energy dispersive x-ray spectroscopy (EDX). The TEM study was conducted on a continuous Au(10 nm)-capped Co(10 nm)/PZT(150 nm) bilayer without micro-patterns. The system was in the as-grown state (no electric field applied).

2. METHODS

Sample design and measurement geometry. Twelve micro-capacitors (150 x 150 μm^2) are fabricated in each sample by means of photolithography to ensure the reproducibility of the results and reliable statistics (Figure 1(a)). The multiferroic heterostrostructure is formed by a thin Co layer (5-10nm) grown at room temperature by means of electron beam-assisted thermal deposition on granular PZT(150 nm or 260 nm) films grown by a sol-gel process on Pt(150nm)/Ti/SiO_2/Si(001) wafers. The surface of the PZT substrate is prepared using oxygen plasma and soft ion bombardment prior to the growth of Co. A 5 nm-thick Au capping layer is deposited on Co to prevent the

magnetic layer from contamination, and to ensure a good electrical contact. The voltage is applied between a Pt base electrode and Au pads (top electrodes) in contact with the Co dots, as shown in Figure 1(a). A 155 nm-thick SiO_2 insulating layer is deposited by magnetron sputtering to reduce the poling area and thereby the leakage current. Two additional samples are further considered as reference systems: A pure ferroelectric sample consisting of Au/PZT/Pt micro-capacitors, and a Co/Au/PZT/Pt sample in which a thin Au layer was interleaved between Co and PZT to suppress interface coupling.

Transmission electron microscopy. The local structure of Co/PZT bilayers is examined by means of transmission electron microscopy (TEM). A Jeol JEM- 2100FS operated at 200 keV is used to record the images and the related chemical mapping by combining the scanning TEM mode (STEM) and energy dispersive x-ray (EDX) spectrometry.

Standard ferroic measurements. We first study the magnetic properties of the Co films using magneto-optical Kerr effect measurements (MOKE), where the Kerr rotation angle $\theta(H)$ is measured in longitudinal geometry. The experimental setup allows applying a DC voltage during the MOKE measurements to study the effect of the electric field on the magnetic anisotropy. The related magnetic moment is obtained by means of superconducting quantum interference device (SQUID) magnetometry measurements and by applying the theoretical sum rules[21,22] to the XMCD data.
The ferroelectric switching is probed with a ferroelectric tester (aixACCT TF 2000E). The polarization loops P(E) are obtained from I(V) measurements through the time integration of the displacement current measured in transverse geometry (Figure 1 (a)). The dynamic P(E) hysteresis measurements provide the basis for the investigation of the characteristic values of the hysteresis loop (P_s, P_r and E_c) in the kHz range. The ferroelectric tester is connected to the optical setup to check possible alterations of the multiferroic device during the magnetoelectric measurements $\theta(E_{AC})$.

Synchrotron-based polarized x-ray absorption spectroscopy. The electronic structure of the interface is further analyzed by means of polarization-dependent soft x-ray absorption spectroscopy (XAS) and magnetic circular dichroism (XMCD). The measurements have been conducted at the French synchrotron facility Soleil, using the cryo-magnet end station of DEIMOS beamline[23]. An ultra-high vacuum preparation chamber (base pressure 10^{-10} mbar) connected to the XAS-XMCD measurement setup has allowed the *in situ* growth of Co ultra-thin films on PZT substrates. The absorption spectra were recorded across the O-K and Ti-$L_{2,3}$ edges in addition to Co-$L_{2,3}$ to investigate both sides of the Co/PZT interface. The absorption spectra are recorded in the total electron yield mode at different incidence angles (30°, 60° and 90° with respect to the film plane) under a magnetic field of 5 T collinear (parallel or antiparallel) to the photons' propagation axis. The polarization of the incident x-rays is reversed at each photon energy point of the absorption spectra to ensure a reduced drift between the scans. One can extract the XMCD signal either from the difference between two

absorption spectra measured at two opposite helicities (left or right circular) for a given magnetic field or, equivalently, by reversing the magnetic field direction at a given handedness of the incident beam. The results presented in this study are obtained in both measurement modes and averaged to reduce possible experimental artifacts.

***Ab-initio* study.** First-principles calculations based on the density functional theory (DFT) were performed using the Vienna Ab initio Simulation Package (VASP)[24,25] with projector augmented wave (PAW) pseudopotentials[26] and the generalized gradient approximation (GGA-PBE)[27]. The energy cutoff of the plane wave basis was fixed at 500 eV and the first Brillouin zone was sampled with a 8x8x3 Monkhorst-Pack grid[28].
We used a 2x2x5.5 $PbZr_{0.25}Ti_{0.75}O_3$(001) cell with a $ZrTi_3O_8$ surface termination, which corresponds to 11 atomic layers in the (001) direction. A single atomic layer of Co has been added at the topmost surface, with 8 Co atoms initially located on top of the oxygen atoms of the $ZrTi_3O_8$ terminated PZT surface. The coordinates of the first 5 PZT atomic layers the farthest from the interface were kept fixed to their bulk value at a given electric polarization state, while the top layers were allowed to relax as described by Fechner *et al.*[29]. The relaxed equilibrium structure near the interface was calculated for both upward and downward polarized PZT in order to study the polarization orientation effect on the electronic structure of the interface (density of states and spin magnetic moments).

Optical measurements of the MEC. The magnetoelectric coupling is investigated by means of electric field-dependent optical reflectivity measurements. Before impinging the sample, a HeNe laser beam is *p*-polarized through a Glan-Thompson polarizer. The polarization of the reflected light is analyzed using a balanced photo-detector fixed on a nano-rotator together with a beam splitter (Wollaston prism). Prior to any measurement, the nano-rotator assembly is set to a position where both channels of the balanced photo-detector have equal intensity (nulling position). The response of the studied sample to external fields leads to a change in the polarization of the reflected laser, and thereby to a detection of a non-zero differential signal in channels A and B of the photodetector. The laser polarization rotation angle θ after reflection is given by the difference divided by the sum of the intensities measured in the two channels $\theta = (A-B)/[2(A+B)]$. This custom-built set-up is fitted to a digital microscope to address each micro-capacitor individually.
The magnetoelectric coupling statics and dynamics are studied by measuring the polarization rotation of the reflected light as a function of the external electric field $\theta(E_{AC})$. A function generator is used to produce a maximum voltage of 10 V with a triangular or sinusoidal waveform ranging from DC to 30 MHz with 1 µHz resolution. A high-speed data acquisition card allows for the simultaneous acquisition of 4 channels (typically, A, B, A-B and the applied field) at 2.5 MHz with 14 bit precision requiring nominally a streaming speed of 140 Mbps. The data is saved and read back immediately for processing, thereby avoiding memory overflow. Constant availability of this read/write speed is ensured by the use of two solid-state drives with write/read speeds

above 200 MBps. The polarization rotation $\theta(E_{AC})$ is directly related to the optical polarization contrast, *i.e.*, to the electric field-driven magneto-optical response due to the MEC and to the electro-optical effect of the ferroelectric subcomponent. These two effects are identified and their contributions disentangled from the overall optical signal, as explained in the following.

The electric-field modulation of θ allows for a direct probe of the converse magnetoelectric coupling. The combination of the fast electric sweep and the rapid data acquisition system enables us to ensure:

- High precision measurements, as variations of the order of 0.05 mrad could be easily resolved in dynamic measurements. This is a significantly higher resolution than ~ 0.25 mrad in static MOKE;
- The possibility to study dynamic effects related to the rate of the electric field sweep;
- The minimization of the Joule effect related to leakage currents. The dynamic measurement thereby reduces the possible deterioration of the metal/oxide interface during the measurements and thus increases the lifetime of the magnetoelectric device.

3. RESULTS AND DISCUSSION

Panel (c) of Figure 1 shows, on the left-hand side, the STEM image of a cross section of typical Co/PZT bilayers with the stacking Au(10nm)/Co(10nm)/PZT(150nm)/Pt(150nm). The right-hand side of the image shows the corresponding layer-resolved chemical analysis. The Co layer forms a continuous film that perfectly follows the granular topography of the textured tetragonal PZT film. The maximum surface roughness of the films is of about 2 nm.

The analysis of the interface structure using high-resolution TEM reveals the existence of nanocrystals in the cobalt layer (Figure 1(b)-(c)). Remarkably, the whole sample shows the same bright region at the Co/PZT interface (highlighted by an arrow in Figure 1(b)). We attribute this contrast to a ~1 nm thick region that could be related to a different atomic environment of Co at the interface. This could be ascribed either to Co-O bonds or to a change in the lattice constant of Co (*i.e.*, local variations of the nearest-neighbor Co-Co distance) close to the interface with respect to the bulk (inside the film, at larger distance from the interface). The latter observation would imply changes in the Co-Co radial distribution near the interface, as it has been reported in a theoretical study by Borisov *et al.*[18].

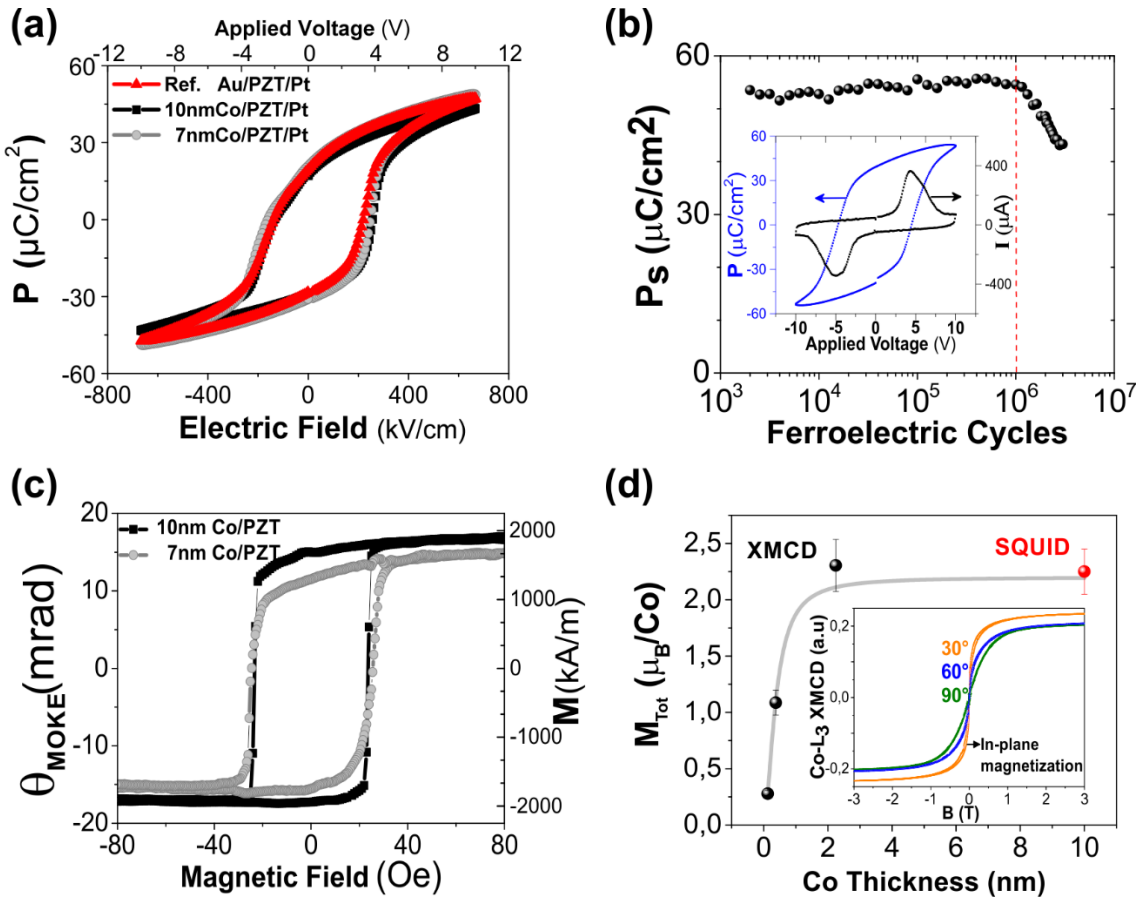

Figure 2. Multiferroic properties at room temperature. (a) Ferroelectric P(E) loops and (b) fatigue effect measured at 1 kHz. The magnetic hysteresis loops are measured by means of (c) longitudinal MOKE in Au(5nm)-capped Co(7-10nm)/PZT(150nm) bilayers. The limits of the scale on the right-hand side represent the saturation magnetization measured with a SQUID magnetometer. (d) Co thickness-dependent in-plane magnetization measured by means of XMCD at 250 K and 5 T (black dots). The experimental point at 10 nm (red) corresponds to the magnetic moment measured by means of SQUID. The inset displays magnetic hysteresis loops in Co(2.5nm)/PZT(150nm) obtained by recording the XMCD intensity at Co-L_3 edge for different incidence angles of the x-rays (30°, 60° and 90° with respect to the film plane).

The coexistence of the ferroelectric and magnetic orders is first examined by means of standard ferroelectric measurements (P-loops) and MOKE magnetometry (θ(H)). The hysteretic switching of both the magnetization and polarization in Co/PZT bilayers at room temperature is presented in Figure 2(a-c), demonstrating the multiferroicity of the system.

The P-E loops (cf. Figure 2(a)) exhibit a saturation polarization (here at 10 V) of about 55 μC/cm^2 and a remanent polarization of 30 μC/cm^2. We observe similar loops in Au/PZT(150nm)/Pt and Co(7-10nm)/PZT(150nm)/Pt, independent on the thickness or the magnetic character of the electrodes. The fatigue effect has also been investigated in Au/PZT/Pt capacitors to evaluate the influence of the electric field cycling on the alteration of the ferroelectric properties. We find that the saturation polarization (P_s) remains constant over more than a million cycles (electric field sweep frequency range

0.5 - 3 kHz), and afterwards it gradually decreases (Figure 2(b)). The inset in Figure 2(b) shows a typical polarization curve and the corresponding dynamic I(V) loop measured after two million cycles. In the following MEC study, we make sure to remain below half a million measurements per micro-capacitor to avoid fatigue contributions. Also, a maximum voltage of 10 V ($\boldsymbol{E}$ = 666.7 kV/cm) is applied in the static as well as in the dynamic MEC measurements, which is far above the ferroelectric coercivity.

Figure 2(c) displays the characteristic MOKE hysteresis loops obtained in Au(5nm)/Co(5-10nm)/PZT(150nm)/Pt micro-capacitors in the longitudinal geometry (*i.e.*, with sensitivity to the in-plane component of the magnetization). The scale on the right-hand side of the graph displays the corresponding in-plane saturation magnetization measured at 300 K in continuous Au(5nm)/Co(7-10nm)/PZT(150nm)/Pt layers (without micro-patterning) using a SQUID magnetometer. Figure 2(d) shows the strong variation of the cobalt atom magnetic moment when the magnetic film thickness is below 2 nm. This variation is likely related to the topography of the bilayers before the coalescence of the magnetic film, which is strongly influenced by the 3-dimensional growth of Co (small islands) and by the PZT substrate roughness (about 2 nm). Above 2 nm, when a continuous layer of Co is formed on PZT, an average magnetic moment $M_{Tot} \approx 2.2\ \mu_B$/Co is obtained. The magnetic hysteresis loops recorded at the Co-edge in Co(2.5nm)/PZT for different incidence angles of the x-rays (30°, 60° and 90° with respect to the film plane) shows an abrupt magnetization switching and a larger dichroic signal when measured at grazing incidence (inset of Figure 2(d)). This result is consistent with an in-plane easy magnetization. Further magnetic measurements at various azimuth angles did not show any preferential magnetization axis within the film plane.

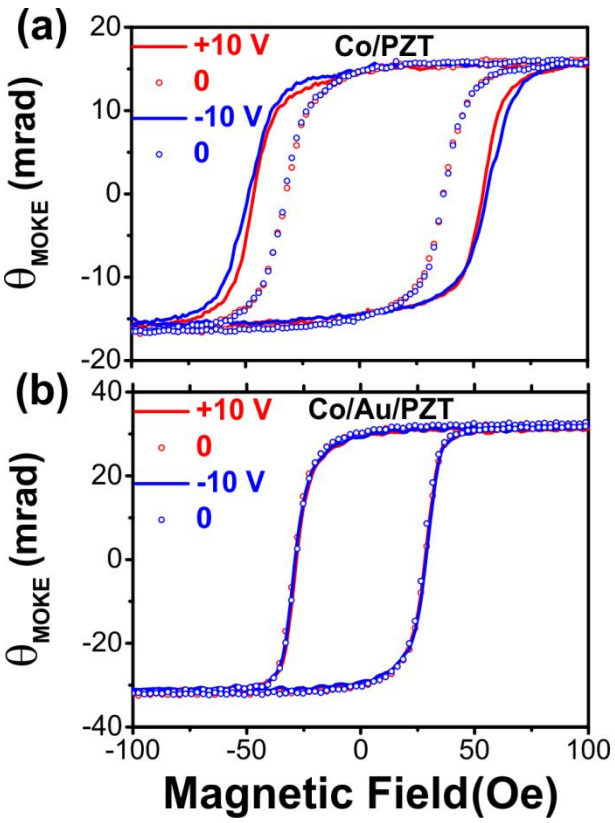

Figure 3. MOKE hysteresis loops with static bias voltage in Au(5nm)-capped (a) /Co(10nm)/PZT and (b) Co(10nm)/Au(8nm)/PZT.

We first study the MEC in static mode, by exploring the effect of a DC bias voltage on the magnetic hysteresis loops. A clear and reversible variation of the magnetic hysteresis loop is observed upon application of a static voltage V_{DC} = ±10 V. In particular, the coercive field increases from 34 Oe at zero DC bias to 51 Oe when the voltage is applied (Figure 3(a)). Yet, no significant variation of the MOKE rotation (magnetization) with the electric field could be detected within the resolution limit (about 5%) in static MOKE measurements. The electric field-induced magnetic anisotropy could not be connected to a macroscopic magnetization reorientation. Remarkably, the electric field-induced change of the magnetic anisotropy vanishes when a thin gold layer is interleaved between Co and PZT (Figure 3(b)). This result suggests that the interface magnetization is affected by local electric fields.

The electric field-induced magnetization tuning at the interface between a ferromagnetic metal or a magnetic semiconductor and an adjacent insulating layer is usually assigned to a spin-dependent charge screening effect[30,31]. However, when the insulating oxide is ferroelectric, the atomic distance between the cation and the ferromagnetic nearest neighbors at the interface varies upon polarization reversal. Thus, the polarization switching changes the overlap between the electron orbitals and consequently modifies the electronic structure at the interface[32–35]. The element and orbital sensitivity of XMCD or resonant magnetic scattering are highly suited tools for the experimental

detection of this interface bonding mechanism and orbital reconstruction[36–38]. We investigate the Co/PZT interface electronic structure in a joint experimental and theoretical approach, where the magnetic moments are measured experimentally (XAS-XMCD) and compared to the calculated values (DFT).

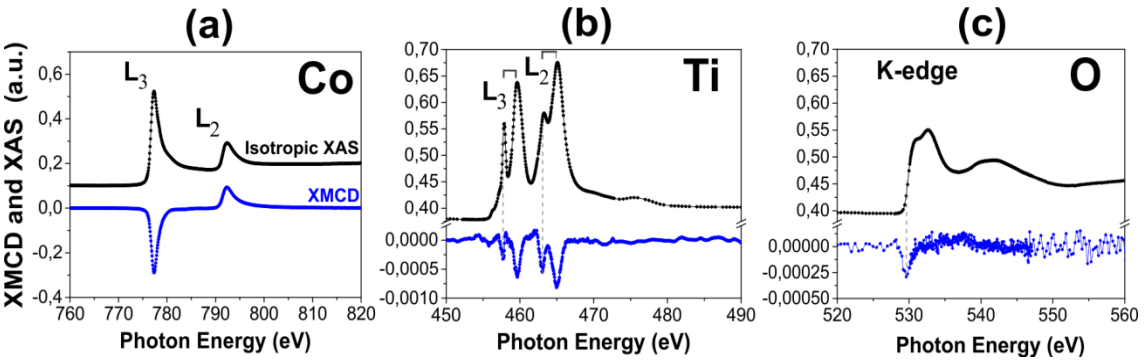

Figure 4. Isotropic XAS and the related XMCD signal measured in Co(2.5nm)/PZT at the (a) Co-$L_{2,3}$, (b) Ti-$L_{2,3}$, and (c) O-K edges in Co(2.5nm)/PZT. The measurements were recorded at 250 K and a magnetic field of 5 T was applied at 30° with respect to film plane (collinear to the incident photons).

The XAS-XMCD measurements are conducted in Co ultra-thin films grown *in situ* on tetragonal PZT substrates containing c-type domains (80-100 nm wide) in which the electric polarization is perpendicular to the surface. Probing the x-ray absorption edges of Co, Ti and O atoms allows us to examine both, the ferromagnetic top layer and the surface of the ferroelectric substrate (*cf.* Figure 4(a-c)). Remarkably, a clear XMCD response is also detected at the Ti-$L_{2,3}$ (Figure 4(b)) and O-K (Figure 4(c)) edges, revealing the existence of magnetic moments in the otherwise non-magnetic PZT layer. It is also noteworthy that the absorption spectra measured at the Ti $L_{2,3}$-edges exhibits a predominant Ti^{4+} character. However, a small contribution of Ti^{3+} ions cannot be excluded since the XAS associated with this component exhibits broad peaks and a small signal that is difficult to separate from the dominating Ti^{4+} component[39].

To investigate more precisely the impact of the direction of the ferroelectric polarization on the electronic structure of Co and PZT at the interface, we employed first-principles calculations based on the DFT. Figure 5(a) displays the atomic structure of the topmost section of the calculated supercell, highlighting the Co/PZT interface for two opposite polarization states after relaxation of the atomic positions. We assume that the first Co atomic layer in contact with PZT governs the interface-related coupling. We therefore consider a single layer of Co on PZT in the calculations, an approach which is also in agreement with a recent study by Borisov *et al.* showing the localized character of MEC[18].

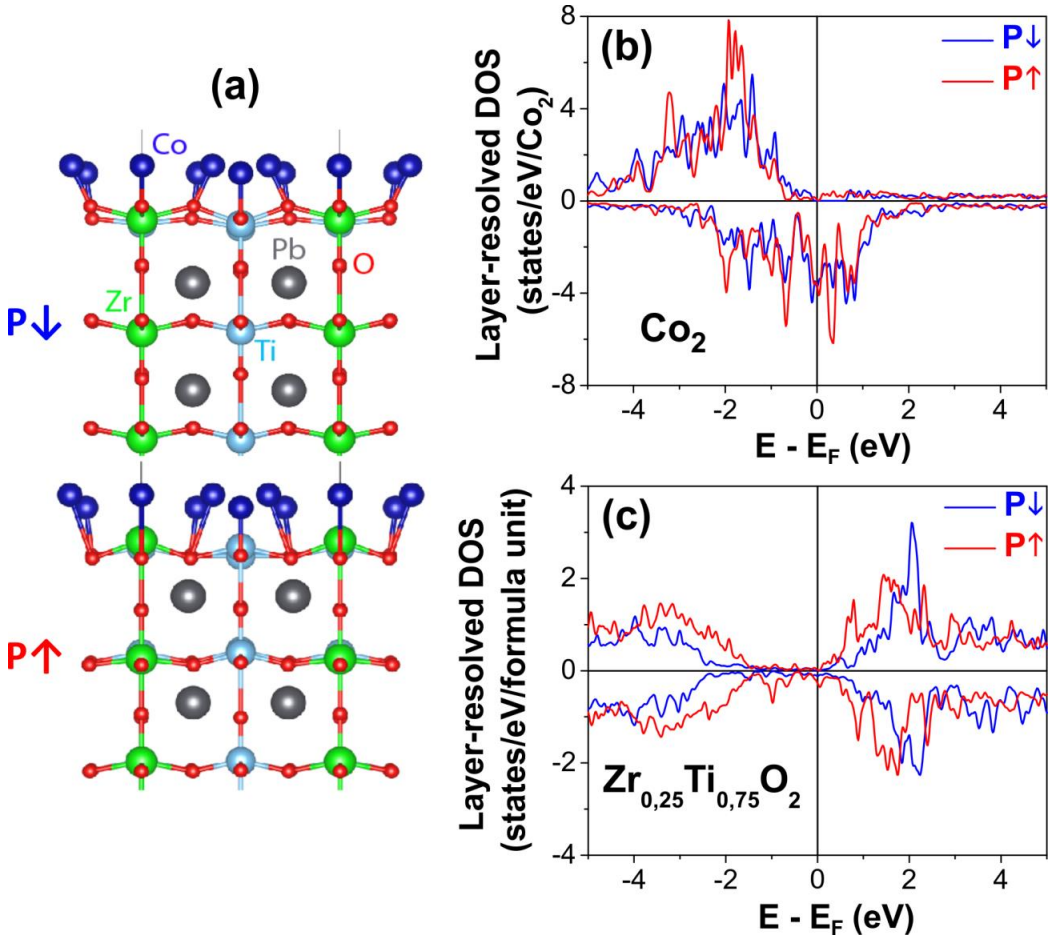

Figure 5. (a) Atomic structure of the 5 topmost atomic layers of $Pb(Zr_{0.25},Ti_{0.75})O_3$ and the Co monolayer for two opposite polarization states. Layer-resolved total density of states per formula units of the (b) Co_2 layer and of (c) the $Zr_{0.25}Ti_{0.75}O_2$ –terminated interfacial layer.

The Co-O distance varies from 1.914 Å to 2.022 Å or from 1.857 Å to 2.790 Å upon polarization reversal from downward to upward, depending on the in-plane environment of the oxygen atoms (Ti-O-Ti or Ti-O-Zr, respectively). We observe a lateral displacement of Co in the [100] or [010] directions with respect to the cubic face centered primary structure (*i.e.*, before relaxation, where the Co atoms are on top of oxygen atoms). The amount of this lateral displacement of Co (from Zr towards Ti) also depends on the polarization direction. We obtain a variation of 0.751 Å for downward polarization, and 0.879 Å for upward polarization.

The calculated density of states (DOS) displayed in Figure 5(b) clearly shows the effect of the polarization direction on the interface electronic structure. Moreover, hybridization occurs between O *p* and Co *d* states and between the *d* states of Co and Ti, which induces a magnetic moment in the otherwise non-magnetic $Zr_{0.25}Ti_{0.75}O_2$ surface. We attribute this induced magnetic moments in O and Ti to their atomic proximity to Co and thus to the polarization orientation (Table 1). The spin magnetic moment of Ti is thus larger for upward than downward polarization direction, but its sign remains opposite to that of Co atoms, regardless of the polarization direction. To corroborate this

result, it is possible to extract the spin moment value from the experimental measurements by applying the well-known sum rules to the XMCD data. However, the quantitative value of the spin moment measured at the Ti L-edge is inaccurate. This is due to the overlap of L_2 and L_3 edges (small energy difference) in light 3*d* metals[40]. In spite of the inaccuracy of the quantitative value of the spin moment at the Ti *L*-edge, the sign reversal between Co and Ti could be examined qualitatively. To do so, the integral of the XMCD signal over L_3 edge (p) and the integral over L_3+L_2 edges (q) involved in the spin moment sum rule are compared for Co and Ti. The (effective) spin moment sum rule is given by: $m_s \approx -(3p-2q)$. In the case of Co, $p > (2/3)q$ leads to a positive spin moment. At the Ti edge, $p < (2/3)q$, means that the spin moment of Ti is reversed with respect to Co. A similar result has been reported in $BiMnO_3/SrTiO_3$, where antiparallel orientation of Ti and Mn magnetic moments at the interface was evidenced by XMCD[39].

		P↓	**P↑**
m_S (μ_B/atom)	**Co**	2.05	1.82
	Ti	-0.05	-0.40
	Zr	0.03	-0.04
	O	0.10	0.03
d Co-O (Å)	**Ti-O-Ti**	1,914	2,022
	Zr-O-Ti	1,857	2,790

Table 1. Variation of the spin magnetic moments and the interatomic Co-O distances upon polarization orientation reversal from upward (P↑) to downward (P↓) obtained by means of first-principles calculations.

The change of the spin moments of Co, O and Ti upon polarization reversal (Table 1) is linked to the modification of the electronic bonding at the interface between Co and PZT. This result is in perfect agreement with a theoretical study reported in Ref.[18] and with our XMCD data, showing a clear magnetic moment carried by Ti and O atoms in Co(2.5 nm)/PZT bilayers and antiferromagnetic coupling between Ti and Co.

A more detailed exploration of the MEC in Co/PZT requires further experimental investigations on the effect the electric field on the surface magnetization. Standard MOKE measurements under static voltage are particularly sensitive to magnetic anisotropy and macroscopic spin reorientation transitions, but they are much less sensitive to tiny variations of the magnetization at buried interfaces. The direct probe of the MEC is better addressed by dynamic measurements in which the optical signal is modulated by an AC electric field (*cf.* details in the METHODS section).

Several studies based on dynamic MOKE experiments have evidenced the electric field modulation of the reflected light polarization in ferroelectric/ferromagnetic (FE/FM) bilayers even in the absence of an applied magnetic field[15,41]. It should however be kept in mind that the electric field-induced optical response in multiferroic heterostructures can be very intricate. For example, in $PbZr_{0.2}Ti_{0.8}O_3/La_{0.8}Sr_{0.2}MnO_3$ bilayers, in which charge mediated coupling has been demonstrated to be the sole coupling mechanism[42], regular square θ(E) hysteresis loop are obtained[15,43], whereas complex asymmetric butterfly-like loops have been reported in other systems[44,45], in which different coupling mechanisms could coexist[46]. More importantly, the electric field-induced birefringence of the ferroelectric subcomponent may also contribute to the overall optical signal.[47] These complications render the unambiguous interpretation of measurements arduous.

In our optical study of the MEC in Co/PZT bilayers, we address the possibility to disentangle the interface-located MEC component among other possible contributions. In particular, we consider the influence of the electric field-dependent birefringence of the ferroelectric layer on the optical response (reflectance and polarization rotation) and we propose a general procedure for distinguishing between different optical components. This possibility allows for the specific study of the magnetoelectric hysteresis loops and their dynamics.

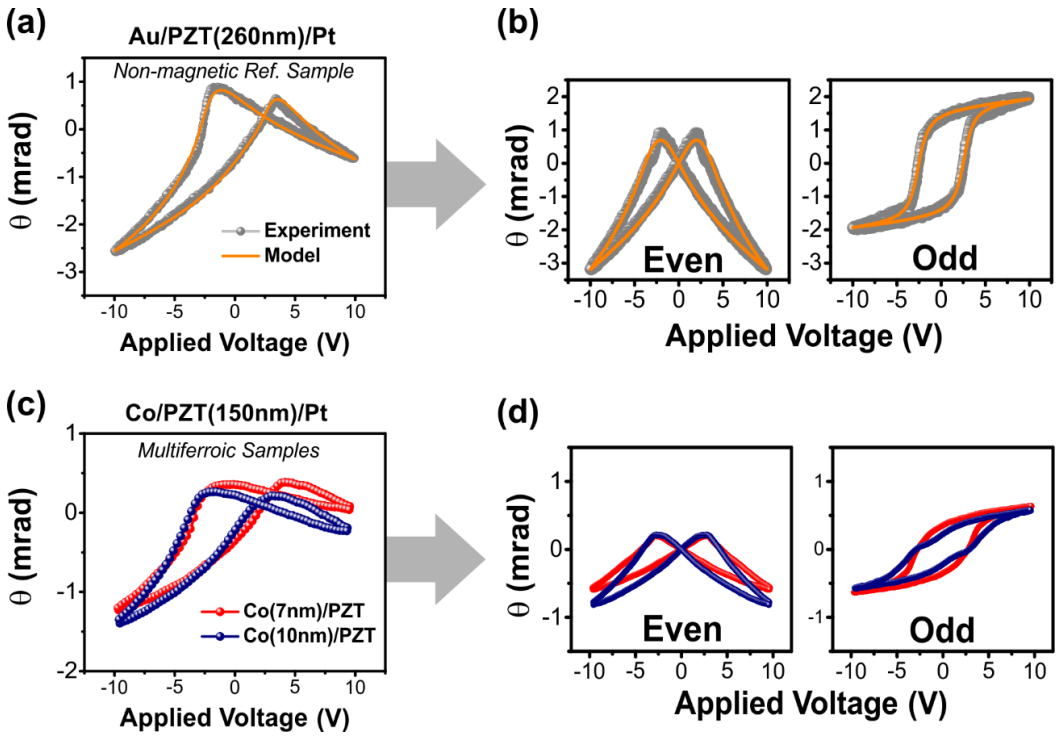

Figure 6. Voltage-induced polarization rotation of the reflected light measured without applied magnetic field in (a) Au(10nm)/PZT(240nm)/Pt(150nm) micro-capacitors subject to a sinusoidal electric field swept at 2 kHz and in (c) Au(5nm)/Co(7-10nm)/PZT(150nm)/Pt(150nm) micro-capacitors subject to a sinusoidal electric field swept at 3 kHz; (b-d) Decomposition of the as-measured signal into an even (left) and odd (right) symmetry components with the applied voltage following the method detailed in the text.

In order to quantify the optical contribution of the ferroelectric layer to the polarization rotation of the reflected light in Co/PZT bilayers, we measure a purely ferroelectric Au/PZT(240nm)/Pt micro-capacitor as a reference sample. The experimental data are represented by gray dots in Figure 6(a). Interestingly, the optical response θ(E) of the reference sample shows a hysteretic variation with the electric field and an asymmetric butterfly-like shape. Figure 6(c) shows that the multiferroic Co/PZT/Pt micro-capacitors also exhibit comparable asymmetric butterfly-like θ(E) hysteresis loops. This result proves that the electric field modulated optical response in FE/FM bilayers as-measured with a MOKE setup is not solely related to the MO Kerr effect (*i.e.*, to the magnetization-related component induced by the MEC). An optical response arising from the ferroelectric oxide layer also contributes to the θ(E) signal and should be considered in the evaluation of MEC. The non-magnetic component is attributed to the electro-optical effect (EO) that results from the change of the refractive indices of the material (*i.e.*, changes in the optical dielectric permittivity tensor) with the applied electric field. This electric field-induced birefringence leads to a phase and amplitude change in the reflected or transmitted optical signal, as demonstrated in various ferroelectric materials, including $BiFeO_3$[48], $BaTiO_3$[49], $(Pb,La)(Zr,Ti)O_3$[50] and $Pb(Zr,Ti)O_3$[51].

The variation of the index of refraction Δn can be represented by the sum of linear and quadratic components with the electric field $\boldsymbol{E}$, known as Pockels effect (linear EO effect) and EO Kerr effect, respectively[52]:

$$\Delta\,(1/n_{ij}^2) = (r_{ijk} + p_{ijl}d_{ljk}\,)\,\boldsymbol{E_k} + (R_{ijkl} + p_{ijmn}M_{mnkl})\,\boldsymbol{E_k E_l} \qquad (1),$$

were r_{ijk} and R_{ijkl} are the strain-free Pockels and EO Kerr coefficients. In the low-frequency regime (sub-GHz), the strain induced by the piezoelectric effect and electrostriction affects also the refractive indexes through the elasto-optic coupling. Therefore, strain related factors containing the elasto-optic coefficients (p_{ijl}), the piezoelectric and the electrostriction tensors elements (d_{ijk} and M_{mnkl}, respectively) are implemented in equation (1). The corresponding optical dielectric permittivity tensor takes the following form in tetragonal PZT (4*mm* point group symmetry) for an applied electric field along the optical axis:

$$\varepsilon = \begin{pmatrix} (n_o - {}^1\!/_2\, n_o^3(r'_{13}E + s'_{12}E^2))^2 & 0 & 0 \\ 0 & (n_o - {}^1\!/_2\, n_o^3(r'_{13}E + s'_{12}E^2))^2 & 0 \\ 0 & 0 & (n_e - {}^1\!/_2\, n_e^3(r'_{33}E + s'_{11}E^2))^2 \end{pmatrix} \qquad (2),$$

were $n_{o(e)}$ are the ordinary or extraordinary components of the index of refraction, and

$$r'_{13} = r_{13} + d_{31}(p_{11} + p_{12}) + d_{33}p_{13},$$
$$r'_{33} = r_{33} + 2p_{13}d_{31} + d_{33}p_{33},$$
$$s'_{12} = s_{12} + M_{12}(p_{11} + p_{12}) + M_{11}p_{13},$$

$$s'_{11} = s_{11} + M_{12}(p_{13} + p_{13}) + M_{11}p_{33}.$$

We model the propagation of the electromagnetic wave through the ferroelectric micro-capacitor taking into account the optical permittivity tensor of tetragonal PZT (Equation (2)) and its electric-field dependence. Because of the birefringence of the medium, mode coupling appears at the Au/PZT/Pt interfaces, leading to four complex amplitudes of the electric field associated with the incident and reflected light ($\boldsymbol{E}^{(i)}$ in Equation (3)) and four complex electric field amplitudes associated with the transmitted wave ($\boldsymbol{E}^{(t)}$ in Equation (3)). Therefore, we use a 4x4 transfer matrix formalism to treat the electromagnetic wave propagation in the birefringent layered media[53,54]. The complex electric field amplitudes of the electromagnetic wave are related through the transfer matrix as follows:

$$\begin{pmatrix} E_s^+ \\ E_s^- \\ E_p^+ \\ E_p^- \end{pmatrix}^{(i)} = \begin{pmatrix} T_{11} & T_{12} & T_{12} & T_{14} \\ T_{21} & T_{22} & T_{23} & T_{24} \\ T_{31} & T_{32} & T_{33} & T_{34} \\ T_{41} & T_{42} & T_{43} & T_{44} \end{pmatrix} \begin{pmatrix} E_s^+ \\ 0 \\ E_p^+ \\ 0 \end{pmatrix}^{(t)} \quad (3),$$

were T_{ij} are the transfer matrix elements, the s and p indexes represent the polarization of the light, + describes the incident (along the propagation direction) and – the reflected electric field components of the light.
The reflection Fresnel coefficients (r_{ij}) related to the experimentally accessible reflectance (R) and the polarization rotation (θ) are calculated from the elements of the transfer matrix as follows[54]:

$$r_{pp} = \left(\frac{E_{p-}^{(i)}}{E_{p+}^{(i)}}\right)_{E_{s+}^{(i)}=0} = \frac{T_{11}T_{43} - T_{41}T_{13}}{T_{33}T_{11} - T_{13}T_{31}} \quad (4),$$

$$r_{ss} = \left(\frac{E_{s-}^{(i)}}{E_{s+}^{(i)}}\right)_{E_{s+}^{(i)}=0} = \frac{T_{21}T_{33} - T_{23}T_{31}}{T_{33}T_{11} - T_{13}T_{31}} \quad (5),$$

$$r_{sp} = \left(\frac{E_{p-}^{(i)}}{E_{s+}^{(i)}}\right)_{E_{p+}^{(i)}=0} = \frac{T_{41}T_{33} - T_{43}T_{31}}{T_{33}T_{11} - T_{13}T_{31}} \quad (6),$$

$$r_{ps} = \left(\frac{E_{s-}^{(i)}}{E_{p+}^{(i)}}\right)_{E_{s+}^{(i)}=0} = \frac{T_{11}T_{23} - T_{21}T_{13}}{T_{33}T_{11} - T_{13}T_{31}} \quad (7).$$

All the optical properties measured in reflection detection mode can be calculated from equations (4-7). The reflectance for p- and s-polarized light (*i.e.* the two components of the reflected light measured in the balanced photodetector) are given by $R_p = (r_{pp})^2$ and $R_s = (r_{ss})^2$. The rotation of the incident p-polarized light upon reflection is obtained from the Jones' formalism[55], representing the rotation θ of a linear analyzer as follows:

$$\begin{pmatrix} \cos^2\theta & \cos\theta\sin\theta \\ \cos\theta\sin\theta & \sin^2\theta \end{pmatrix} \begin{pmatrix} r_{ss} & r_{sp} \\ r_{ps} & r_{pp} \end{pmatrix} \begin{pmatrix} 0 \\ 1 \end{pmatrix}$$

$$= \left(r_{sp}\cos\theta + r_{pp}\sin\theta\right)\begin{pmatrix}\cos\theta\\ \sin\theta\end{pmatrix} \qquad (8),$$

For θ << 1 at the nulling state (where the two components of the reflected light are balanced in the two detectors) we obtain:

$$\theta \approx Re\left\{-\frac{r_{sp}}{r_{pp}}\right\} \qquad (9)$$

In order to model the electric field-dependence of the optical response of the ferroelectric reference sample, it is important to note that the EO effect depends on the internal electric field (*i.e.*, on the field sensed by the system) which consists of a combination of the applied field and the dipolar field in the sample. In the case of plane capacitor samples, the dipolar field is proportional to the ferroelectric polarization[56] and it has thus the same hysteretic variation with the applied field. The dipolar field is simulated by a slowly varying arctangent function[57] taking into account the saturation polarization and the coercivity obtained from the experimental P(E) measurements (Figure 2(a)). The numerical values of the elasto-optic, piezoelectric and the electrostriction coefficients are taken from the literature for tetragonal $BaTiO_3$[58] which is known to exhibit comparable physical proprieties as tetragonal PZT.

The validity of the model is confirmed by closely fitting the optical experimental data as shown in Figure 6 (continuous line). This result shows that the overall electric-field-dependent optical response of the purely ferroelectric reference sample is fully accounted for with a combination of Pockels and EO Kerr effects (Figure 6 (a,b)). Therefore, we expect the coexistence of both EO and MO effects in Co/PZT bilayers and emphasize the importance of eliminating the EO component in MEC studies as explained below.

The electric field-dependent physical properties that can change the polarization of the reflected light (*e.g.*, EO and MO effects) can be separated according to their dependence on the direction of the applied electric field. Therefore it is convenient to separate the optical components of odd (quadratic) from those of even symmetry (linear) with respect to ***E***. The separation of the odd and even components is achieved by using a numerical decomposition of the experimental data. If "i" denotes the signal with increasing field ***E***, and "d" the signal with decreasing field, the odd increasing branch is 0.5(i(*E*) -d(-*E*)) and the even increasing branch is 0.5(i(***E***) +d(-***E***)). Similarly, the odd decreasing branch is 0.5(d(***E***) -i(-***E***)) and the even decreasing branch 0.5(i(-***E***) +d(***E***)). The as-extracted odd (square loops) and even components (butterfly-like loops) are displayed in Figure 6 (b,d).

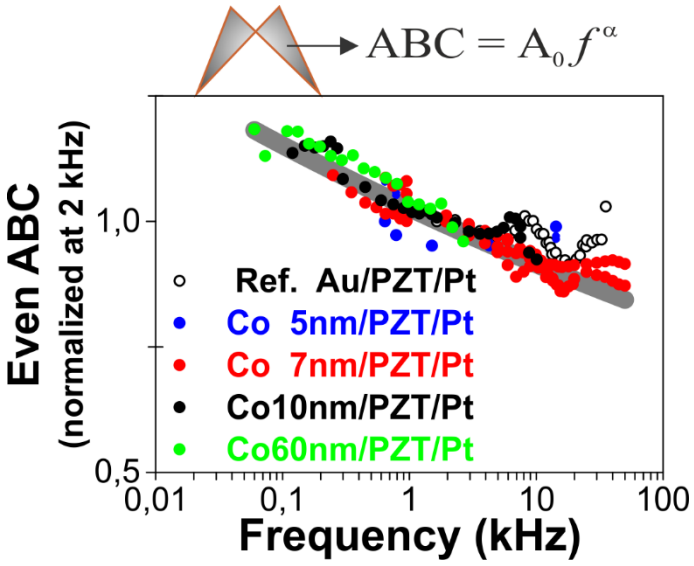

Figure 7. Frequency dependence of the Area Between the Curves (ABC) having an even symmetry with the electric field. This area is indicated by the gray region in the schematically represented butterfly-like loop. The curves are normalized by their values at 2 kHz.

Figure 7 shows the Area Between the Curves (ABC) of even symmetry, calculated by numerical integration of the area enclosed by the butterfly-like hysteresis loops, as a function of the frequency (*f*). Interestingly, the same variation is observed in the multiferroic micro-capacitors as well as in the purely ferroelectric reference sample. The ABC is fitted with a common function $A_0 f^{\alpha}$ (continuous line in Figure 7), were A_0 is a constant. A dynamic scaling as $f^{\alpha}E^{\beta}$ has been reported in ferroelectric P(E) hysteresis loop area in different ferroelectric materials (see Ref. [59] and references therein). This result suggests that the even component in Co/PZT bilayers is related to the birefringence of the PZT layer, and thus to the ferroelectric properties of the ferroelectric layer. Therefore, EO optical measurements can be regarded as an alternative way to probe the polarization switching as reported on PZT by Potter *et al.*[51]. The decrease of the even ABC intensity characterized by a negative scaling factor α = -0.09 (Figure 7) indicates a slow-down of the domain dynamics. This is probably due to incomplete compensation of the depolarization field at high-frequencies.

To obtain the MO component purely related to MEC, the signal arising from the electric field-induced birefringence should be removed. This can be achieved by subtracting the optical response of the ferroelectric substrate alone from the data measured in FM/FE bilayers. However, several precautions should be considered. First, the ferroelectric layer in the two samples should have the same characteristics in terms of thickness and ferroelectric properties. Second, the two samples must be measured under the same experimental conditions. In particular, the acquisition time, the number of measured cycles and the frequency of the applied field may affect both the signal intensity and the coercivity values. Lastly, a correction factor should be applied before subtraction to

account for the reflectivity difference between the top electrodes in the two samples (Au(15nm) in the reference sample, and Au(5nm) + Co(2-10nm) in the bilayers).

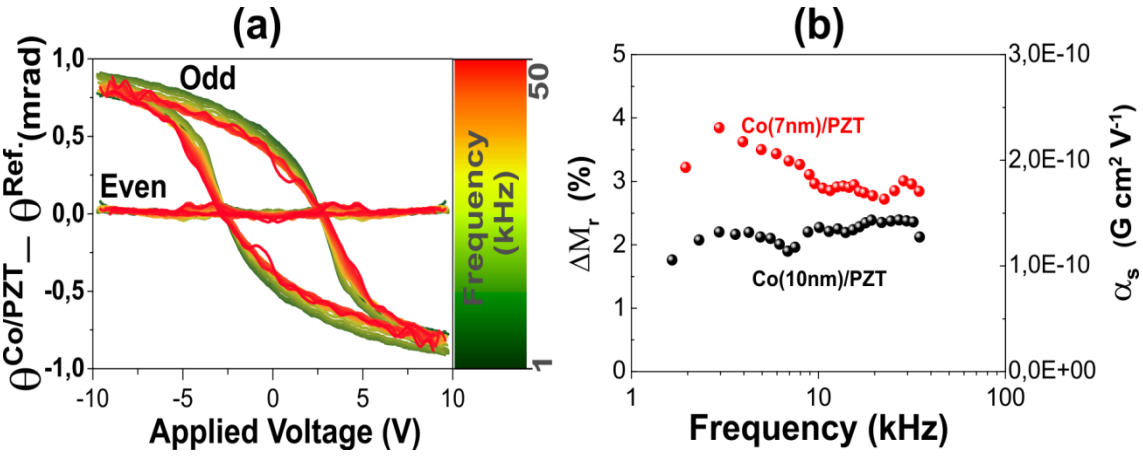

Figure 8. (a) Odd and Even hysteresis loops measured in Co(7nm)/PZT after the removal of the purely EO contributions of the PZT reference sample. The scale on the right-hand- side corresponds to the frequency at which the electric field is swept. (b) Surface MEC dynamics representing the evolution of the remanent magnetization fraction (left axis) and the surface magnetoelectric coupling coefficient α_s (right axis).

The result after the removal of the EO component is displayed in Figure 8. We observe that the even symmetry (butterfly-like curves) vanishes after subtraction of the PZT signal, which leads to a MO signal of purely odd symmetry *i.e.*, a square MO hysteresis loop is obtained in Co/PZT bilayers. The resulting MO component at 10 V represents about 5% of the maximum MOKE rotation measured in Co(10nm)/PZT (Figure 2(c)). This corresponds to a magnetization of 1 to 2 atomic layers of Co, which is consistent with interface magnetization. The properties of interface-mediated coupling can thus be deduced from the as-subtracted magnetoelectric curve (odd component, *cf.* Figure 8(a)).

The interface-related MEC factor is defined by the size of the magnetoelectric loop. It is written as $\alpha_s = \mu_0 \Delta M/(tE_c)$, where ΔM is the variation of interface magnetization upon the ferroelectric polarization reversal and t is the thickness of the interface layer involved in the coupling. Given that the remanent magnetization is the main effect in interface-mediated coupling, we consider the variation of the remanence ΔM_r in the estimation of α_s. Figure 8(b) displays the frequency dependence of the remanent surface magnetization fraction defined as $\Delta M_r = \theta_r(E)/\theta_r(H)$. Knowing the correspondence between MOKE rotation and the magnetization measured by means of XMCD and SQUID magnetometry, the quantitative value of the magnetoelectric coupling can be deduced at any frequency. While 7nm-thick Co/PZT shows a slightly larger magnetoelectric coupling than 10 nm-thick Co/PZT, both samples exhibit a coupling of 1-2 $x10^{-10}$ G cm^2/V. This value is comparable to the values reported in the case of $Fe/BaTiO_3$ ($2.2x10^{-10}$ G cm^2/V)[32] and $Fe_3O_4/BaTiO_3$ ($0.7x10^{-10}$ G cm^2/V)[35].

Unlike the ferroelectric material-related dynamics discussed earlier, interface coupling in Co/PZT bilayers exhibits high stability over a wide frequency range of 1-50 kHz. A MEC decay of about 70% has been reported between 1 and 10 Hz in Metglas® ribbons fixed on magnesium niobate-lead titanate crystals, where the coupling is known to be strain mediated[60].

Our study has established the role of the ionic displacement upon polarization reversal on the coupling, which leads to a change in the interface magnetization through a proximity effect at the Co/PZT interface. Yet, other contributions such as effects related to the magnetic configuration at the interface and the possible existence of interfacial phase transitions mediated by Co-O bonds[61–63] represent interesting topics which could be further explored in future studies.

4. CONCLUSIONS

Room temperature multiferroicity and interface-related MEC were evidenced in Co/PZT bilayers. Static MOKE measurements reveal a clear influence of electric fields on the magnetic anisotropy, which results in an increase of about 80% of the coercive field upon application of a static electric field. Dynamic optical measurements display a mixed linear and quadratic optical response to the AC electric field which results from a magneto-electro-optical effect. In particular, quadratic and linear electro-optical effects arising from the ferroelectric PZT layer are found to significantly contribute to the overall response of the Co/PZT bilayers. A signal decomposition method is proposed to separate the EO and the MO components, which allows for a precise investigation of the MEC. A magnetoelectric coupling constant of 1-2x10^{-10} G cm^2/V is obtained in Co(5-10nm)/PZT bilayers when the electric field is swept at 1-50 kHz.

The electronic origin of the coupling has been established through first-principles calculations. The variation of the spin moments carried by Co, O and Ti atoms depending on the polarization direction of the PZT film is related to the modification of the electronic bonding at the interface between Co and PZT. A magnetic dichroism signal of 0.16% and 0.06% of the XAS signal is measured, respectively, at the Ti L-edge and at the O K-edge, revealing the existence of an induced-magnetization in the ferroelectric layer.

The surface-mediated coupling in Co/PZT allows for the electric-field tuning of the magnetization between two non-volatile states, where each state is connected to two opposite ferroelectric polarization orientations (square hysteresis). The possibility to induce effective interface-mediated MEC at room temperature in granular systems opens new prospects towards low-cost manufacturing of magnetoelectric memories and spintronic devices.

AUTHOR INFORMATION

Corresponding Author

***** E-mail: Salia.Cherifi@ipcms.unistra.fr

Notes

The authors declare no competing financial interest.

ACKNOWLEDGEMENTS

This work is supported by the French National Research Agency (ANR) through JCJC program "*DYNAMECS"* ANR-11-JS10-009-01 and the TEM study was conducted in the framework of project "*EMMA"* ANR-12-BS10-013. Financial support by the Spanish Government for the CSIC JAE-predoc grant of O.V. is acknowledged. S. C.-H. acknowledges the technical assistance of J.-S. Pelle (IPHC, Strasbourg) and the team of the STnano cleanroom facility in Strasbourg for the optimization of the magnetoelectric micro-devices. R. Cours (CEMES, Toulouse) is acknowledged for his help with the preparation of the sample lamellas for TEM measurements.

REFERENCES

(1) Tsymbal, E. Y. Spintronics: Electric Toggling of Magnets. *Nat. Mater.* **2011**, *11* (1), 12–13.

(2) Matsukura, F.; Tokura, Y.; Ohno, H. Control of Magnetism by Electric Fields. *Nat. Nanotechnol.* **2015**, *10* (3), 209–220.

(3) Vaz, C. A. F.; Hoffman, J.; Ahn, C. H.; Ramesh, R. Magnetoelectric Coupling Effects in Multiferroic Complex Oxide Composite Structures. *Adv. Mater.* **2010**, *22* (26-27), 2900–2918.

(4) Scott, J. F. Applications of Magnetoelectrics. *J. Mater. Chem.* **2012**, *22* (11), 4567.

(5) Scott, J. F. Room-Temperature Multiferroic Magnetoelectrics. *NPG Asia Mater.* **2013**, *5* (11), e72.

(6) Lu, C.; Hu, W.; Tian, Y.; Wu, T. Multiferroic Oxide Thin Films and Heterostructures. *Appl. Phys. Rev.* **2015**, *2* (2), 021304.

(7) Trassin, M. Low Energy Consumption Spintronics Using Multiferroic Heterostructures. *J. Phys. Condens. Matter* **2016**, *28* (3), 033001.

(8) Ma, J.; Hu, J.; Li, Z.; Nan, C.-W. Recent Progress in Multiferroic Magnetoelectric Composites: From Bulk to Thin Films. *Adv. Mater.* **2011**, *23* (9), 1062–1087.

(9) Vaz, C. A. F. Electric Field Control of Magnetism in Multiferroic Heterostructures. *J. Phys. Condens. Matter* **2012**, *24* (33), 333201.

(10) Fernandes Vaz, C. A.; Staub, U. Artificial Multiferroic Heterostructures. *J. Mater. Chem. C* **2013**, *1* (41), 6731.

(11) Garcia, V.; Bibes, M.; Barthélémy, A. Artificial Multiferroic Heterostructures for

an Electric Control of Magnetic Properties. *C. R. Phys.* **2015**, *16* (2), 168–181.

(12) Duan, C.; Jaswal, S. S.; Tsymbal, E. Y. Predicted Magnetoelectric Effect in Fe/$BaTiO_3$ Multilayers: Ferroelectric Control of Magnetism. *Phys. Rev. Lett.* **2006**, *97* (4), 047201.

(13) Rondinelli, J. M.; Stengel, M.; Spaldin, N. A. Carrier-Mediated Magnetoelectricity in Complex Oxide Heterostructures. *Nat. Nanotechnol.* **2008**, *3* (1), 46–50.

(14) Duan, C.-G.; Velev, J. P.; Sabirianov, R. F.; Mei, W. N.; Jaswal, S. S.; Tsymbal, E. Y. Tailoring Magnetic Anisotropy at the Ferromagnetic/ferroelectric Interface. *Appl. Phys. Lett.* **2008**, *92* (12), 122905.

(15) Molegraaf, H. J. a.; Hoffman, J.; Vaz, C. a. F.; Gariglio, S.; van der Marel, D.; Ahn, C. H.; Triscone, J.-M. Magnetoelectric Effects in Complex Oxides with Competing Ground States. *Adv. Mater.* **2009**, *21* (34), 3470–3474.

(16) Garcia, V.; Bibes, M.; Bocher, L.; Valencia, S.; Kronast, F.; Crassous, A.; Moya, X.; Enouz-Vedrenne, S.; Gloter, A.; Imhoff, D.; Deranlot, C.; Mathur, N. D.; Fusil, S.; Bouzehouane, K.; Barthelemy, A. Ferroelectric Control of Spin Polarization. *Science (80-.).* **2010**, *327* (5969), 1106–1110.

(17) Pantel, D.; Goetze, S.; Hesse, D.; Alexe, M. Reversible Electrical Switching of Spin Polarization in Multiferroic Tunnel Junctions. *Nat. Mater.* **2012**, *11* (4), 289–293.

(18) Borisov, V. S.; Ostanin, S.; Maznichenko, I. V.; Ernst, A.; Mertig, I. Magnetoelectric Properties of the Co/$PbZr_xTi_{1-x}O_3$ (001) Interface Studied from First Principles. *Phys. Rev. B* **2014**, *89* (5), 054436.

(19) Borisov, V. S.; Ostanin, S.; Achilles, S.; Henk, J.; Mertig, I. Spin-Dependent Transport in a Multiferroic Tunnel Junction: Theory for Co/$PbTiO_3$/Co. *Phys. Rev. B* **2015**, *92* (7), 075137.

(20) Bowen, M.; Bibes, M.; Barthélémy, A.; Contour, J.-P.; Anane, A.; Lemaître, Y.; Fert, A. Nearly Total Spin Polarization in $La_{2/3}Sr_{1/3}MnO_3$ from Tunneling Experiments. *Appl. Phys. Lett.* **2003**, *82* (2), 233.

(21) Thole, B. T.; Carra, P.; Sette, F.; van der Laan, G. X-Ray Circular Dichroism as a Probe of Orbital Magnetization. *Phys. Rev. Lett.* **1992**, *68* (12), 1943–1946.

(22) Carra, P.; Thole, B. T.; Altarelli, M.; Wang, X. X-Ray Circular Dichroism and Local Magnetic Fields. *Phys. Rev. Lett.* **1993**, *70* (5), 694–697.

(23) Ohresser, P.; Otero, E.; Choueikani, F.; Chen, K.; Stanescu, S.; Deschamps, F.; Moreno, T.; Polack, F.; Lagarde, B.; Daguerre, J.-P.; Marteau, F.; Scheurer, F.; Joly, L.; Kappler, J.-P.; Muller, B.; Bunau, O.; Sainctavit, P. DEIMOS: A Beamline Dedicated to Dichroism Measurements in the 350–2500 eV Energy Range. *Rev. Sci. Instrum.* **2014**, *85* (1), 013106.

(24) Kresse, G.; Hafner, J. Ab Initio Molecular-Dynamics Simulation of the Liquid-Metal–amorphous-Semiconductor Transition in Germanium. *Phys. Rev. B* **1994**, *49* (20), 14251–14269.

(25) Kresse, G.; Furthmüller, J. Efficient Iterative Schemes for Ab Initio Total-Energy Calculations Using a Plane-Wave Basis Set. *Phys. Rev. B* **1996**, *54* (16), 11169–11186.

(26) Blöchl. Projector Augmented-Wave Method. *Phys. Rev. B. Condens. Matter* **1994**, *50* (24), 17953–17979.
(27) Perdew, J.; Burke, K.; Ernzerhof, M. Generalized Gradient Approximation Made Simple. *Phys. Rev. Lett.* **1996**, *77* (18), 3865–3868.
(28) Monkhorst, H. J.; Pack, J. D. Special Points for Brillouin-Zone Integrations. *Phys. Rev. B* **1976**, *13* (12), 5188–5192.
(29) Fechner, M.; Ostanin, S.; Mertig, I. Effect of the Surface Polarization in Polar Perovskites Studied from First Principles. *Phys. Rev. B* **2008**, *77* (9), 094112.
(30) Zhang, S. Spin-Dependent Surface Screening in Ferromagnets and Magnetic Tunnel Junctions. *Phys. Rev. Lett.* **1999**, *83* (3), 640–643.
(31) Duan, C.-G.; Velev, J. P.; Sabirianov, R. F.; Zhu, Z.; Chu, J.; Jaswal, S. S.; Tsymbal, E. Y. Surface Magnetoelectric Effect in Ferromagnetic Metal Films. *Phys. Rev. Lett.* **2008**, *101* (13), 137201.
(32) Duan, C.-G.; Jaswal, S. S.; Tsymbal, E. Y. Predicted Magnetoelectric Effect in Fe/$BaTiO_3$ Multilayers: Ferroelectric Control of Magnetism. *Phys. Rev. Lett.* **2006**, *97* (4), 047201.
(33) Fechner, M.; Maznichenko, I. V.; Ostanin, S.; Ernst, a.; Henk, J.; Bruno, P.; Mertig, I. Magnetic Phase Transition in Two-Phase Multiferroics Predicted from First Principles. *Phys. Rev. B* **2008**, *78* (21), 212406.
(34) Yamauchi, K.; Sanyal, B.; Picozzi, S. Interface Effects at a Half-Metal/ferroelectric Junction. *Appl. Phys. Lett.* **2007**, *91* (2007), 2012–2015.
(35) Niranjan, M. K.; Velev, J. P.; Duan, C.-G.; Jaswal, S. S.; Tsymbal, E. Y. Magnetoelectric Effect at the Fe_3O_4/$BaTiO_3$(001) Interface: A First-Principles Study. *Phys. Rev. B* **2008**, *78* (10), 104405.
(36) Wang, J.; Hu, J.; Wang, H.; Jiang, H.; Wu, Z.; Ma, J.; Wang, X.; Lin, Y.; Nan, C. W. Electric-Field Modulation of Magnetic Properties of Fe Films Directly Grown on $BiScO_3$–$PbTiO_3$ Ceramics. *J. Appl. Phys.* **2010**, *107* (8), 083901.
(37) Valencia, S.; Crassous, A.; Bocher, L.; Garcia, V.; Moya, X.; Cherifi, R. O.; Deranlot, C.; Bouzehouane, K.; Fusil, S.; Zobelli, A.; Gloter, A.; Mathur, N. D.; Gaupp, A.; Abrudan, R.; Radu, F.; Barthélémy, A.; Bibes, M. Interface-Induced Room-Temperature Multiferroicity in $BaTiO_3$. *Nat. Mater.* **2011**, *10* (10), 753–758.
(38) Cui, B.; Song, C.; Mao, H.; Wu, H.; Li, F.; Peng, J.; Wang, G.; Zeng, F.; Pan, F. Magnetoelectric Coupling Induced by Interfacial Orbital Reconstruction. *Adv. Mater.* **2015**, *27* (42), 6651–6656.
(39) Salluzzo, M.; Gariglio, S.; Stornaiuolo, D.; Sessi, V.; Rusponi, S.; Piamonteze, C.; De Luca, G. M.; Minola, M.; Marré, D.; Gadaleta, A.; Brune, H.; Nolting, F.; Brookes, N. B.; Ghiringhelli, G. Origin of Interface Magnetism in $BiMnO_3$/$SrTiO_3$ and $LaAlO_3$/$SrTiO_3$ Heterostructures. *Phys. Rev. Lett.* **2013**, *111* (8), 087204.
(40) Piamonteze, C.; Miedema, P.; de Groot, F. M. F. Accuracy of the Spin Sum Rule in XMCD for the Transition-Metal L Edges from Manganese to Copper. *Phys. Rev. B* **2009**, *80* (18), 184410.
(41) Li, Z.; Hu, J.; Shu, L.; Zhang, Y.; Gao, Y.; Shen, Y.; Lin, Y.; Nan, C. W. A

Simple Method for Direct Observation of the Converse Magnetoelectric Effect in Magnetic/ferroelectric Composite Thin Films. *J. Appl. Phys.* **2011**, *110* (9), 096106.

(42) Vaz, C. A. F.; Hoffman, J.; Segal, Y.; Reiner, J. W.; Grober, R. D.; Zhang, Z.; Ahn, C. H.; Walker, F. J. Origin of the Magnetoelectric Coupling Effect in $PbZr_{0.2}Ti_{0.8}O_3/La_{0.8}Sr_{0.2}MnO_3$ Multiferroic Heterostructures. *Phys. Rev. Lett.* **2010**, *104* (12), 127202.

(43) Vaz, C. A. F.; Segal, Y.; Hoffman, J.; Grober, R. D.; Walker, F. J.; Ahn, C. H. Temperature Dependence of the Magnetoelectric Effect in $PbZr_{0.2}Ti_{0.8}O_3/La_{0.8}Sr_{0.2}MnO_3$ Multiferroic Heterostructures. *Appl. Phys. Lett.* **2010**, *97* (4), 042506.

(44) Li, Z.; Hu, J.; Shu, L.; Gao, Y.; Shen, Y.; Lin, Y.; Nan, C. W. Thickness-Dependent Converse Magnetoelectric Coupling in Bi-Layered Ni/PZT Thin Films. *J. Appl. Phys.* **2012**, *111* (3), 033918.

(45) Shu, L.; Li, Z.; Ma, J.; Gao, Y.; Gu, L.; Shen, Y.; Lin, Y.; Nan, C. W. Thickness-Dependent Voltage-Modulated Magnetism in Multiferroic Heterostructures. *Appl. Phys. Lett.* **2012**, *100* (2), 022405.

(46) Hu, J.-M.; Nan, C.-W.; Chen, L.-Q. Size-Dependent Electric Voltage Controlled Magnetic Anisotropy in Multiferroic Heterostructures: Interface-Charge and Strain Comediated Magnetoelectric Coupling. *Phys. Rev. B* **2011**, *83* (13), 134408.

(47) Shu, L.; Gao, Y.; Hu, J.-M.; Li, Z.; Shen, Y.; Lin, Y.; Nan, C. W. Evaluating the Electro-Optical Effect in Alternating Current-Voltage-Modulated Kerr Response for Multiferroic Heterostructures. *J. Appl. Phys.* **2013**, *114* (20), 204102.

(48) Sando, D.; Hermet, P.; Allibe, J.; Bourderionnet, J.; Fusil, S.; Carrétéro, C.; Jacquet, E.; Mage, J.-C.; Dolfi, D.; Barthélémy, A.; Ghosez, P.; Bibes, M. Linear Electro-Optic Effect in Multiferroic $BiFeO_3$ Thin Films. *Phys. Rev. B* **2014**, *89* (19), 195106.

(49) Abel, S.; Stöferle, T.; Marchiori, C.; Rossel, C.; Rossell, M. D.; Erni, R.; Caimi, D.; Sousa, M.; Chelnokov, A.; Offrein, B. J.; Fompeyrine, J. A Strong Electro-Optically Active Lead-Free Ferroelectric Integrated on Silicon. *Nat. Commun.* **2013**, *4* (6), 1671.

(50) Reitze, D. H.; Haton, E.; Ramesh, R.; Etemad, S.; Leaird, D. E.; Sands, T.; Karim, Z.; Tanguay, A. R. Electro-Optic Properties of Single Crystalline Ferroelectric Thin Films. *Appl. Phys. Lett.* **1993**, *63* (1993), 596–598.

(51) Potter, B. G.; Sinclair, M. B.; Dimos, D. Electro-Optical Characterization of $Pb(Zr,Ti)O_3$ Thin Films by Waveguide Refractometry. *Appl. Phys. Lett.* **1993**, *63* (16), 2180.

(52) Newnham, R. E. *Properties of Materials*; Oxford University Press, Ed.; 2005.

(53) Yeh, P. Electromagnetic Propagation in Birefringent Layered Media. *J. Opt. Soc. Am.* **1979**, *69* (5), 742.

(54) Yeh, P. Optics of Anisotropic Layered Media: A New 4 × 4 Matrix Algebra. *Surf. Sci.* **1980**, *96* (1-3), 41–53.

(55) Yeh, P. Extended Jones Matrix Method. *J. Opt. Soc. Am.* **1982**, *72* (4), 507–513.

(56) Resta, R. Electrical Polarization and Orbital Magnetization: The Modern Theories. *J. Phys. Condens. Matter* **2010**, *22* (12), 123201.

(57) Hejda, P. Simple Representation of Magnetic Characteristics by Smooth Functions. *Czech. J. Phys.* **1985**, *35* (4), 442–458.

(58) Zgonik, M.; Bernasconi, P.; Duelli, M.; Schlesser, R.; Günter, P.; Garrett, M. H.; Rytz, D.; Zhu, Y.; Wu, X. Dielectric, Elastic, Piezoelectric, Electro-Optic, and Elasto-Optic Tensors of $BaTiO_3$ Crystals. *Phys. Rev. B* **1994**, *50* (9), 5941–5949.

(59) Guo, Y. Y.; Wei, T.; He, Q. Y.; Liu, J.-M. Dynamic Hysteresis Scaling of Ferroelectric $Pb_{0.9}Ba_{0.1}(Zr_{0.52}Ti_{0.48})O_3$ Thin Films. *J. Phys. Condens. Matter* **2009**, *21* (48), 485901.

(60) Chen, Y.; Fitchorov, T.; Geiler, A. L.; Gao, J.; Vittoria, C.; Harris, V. G. Dynamic Response of Converse Magnetoelectric Effect in a PMN-PT-Based Multiferroic Heterostructure. *Appl. Phys. A* **2010**, *100* (4), 1149–1155.

(61) Burton, J. D.; Tsymbal, E. Y. Prediction of Electrically Induced Magnetic Reconstruction at the Manganite/ferroelectric Interface. *Phys. Rev. B* **2009**, *80* (17), 174406.

(62) Radaelli, G.; Petti, D.; Plekhanov, E.; Fina, I.; Torelli, P.; Salles, B. R.; Cantoni, M.; Rinaldi, C.; Gutiérrez, D.; Panaccione, G.; Varela, M.; Picozzi, S.; Fontcuberta, J.; Bertacco, R. Electric Control of Magnetism at the $Fe/BaTiO_3$ Interface. *Nat. Commun.* **2014**, *5* (6), 3404.

(63) Spurgeon, S. R.; Balachandran, P. V.; Kepaptsoglou, D. M.; Damodaran, A. R.; Karthik, J.; Nejati, S.; Jones, L.; Ambaye, H.; Lauter, V.; Ramasse, Q. M.; Lau, K. K. S.; Martin, L. W.; Rondinelli, J. M.; Taheri, M. L. Polarization Screening-Induced Magnetic Phase Gradients at Complex Oxide Interfaces. *Nat. Commun.* **2015**, *6*, 6735.